Assessing the Performance of Density Functional Theory for the Electronic Structure of Metal−Salens: The d^6-Metals

Tait Takatani, John S. Sears, and C. David Sherrill*

Center for Computational Molecular Science and Technology, School of Chemistry and Biochemistry, and College of Computing, Georgia Institute of Technology, Atlanta, Georgia 30332-0400

Received: April 27, 2009; Revised Manuscript Received: June 30, 2009

The energies and optimized geometries of the lowest lying singlet, triplet, and quintet states for the Fe(II)−, Co(III)−, Ni(IV)−, Ru(II)−, Rh(III)−, and Pd(IV)−salens have been computed with the B3LYP and BP86 density functional theory (DFT) methods, and the results are compared to more robust complete active-space self-consistent field (CASSCF) values. Density functional optimizations are performed using two different models of the salen ligand, and CASSCF relative energies at these DFT geometries show no appreciable difference whether the smaller or the larger model salen is considered. Unlike in our previous studies on the d^0 and d^2 metal−salens, DFT methods rarely predict the correct ordering of states compared to high-level complete active-space third-order perturbation theory (CASPT3) computations. The DFT energy gaps, moreover, are generally much smaller than those predicted by the CASPT3 method. Similarly to our previous studies, DFT optimized geometries closely match the CASSCF optimized geometries with errors mostly on the order of 0.1 Å least root mean squared deviation. The electronic structure of the Co(III)− and Rh(III)−salens is particularly challenging, and significant differences between CASPT2 and CASPT3 relative energies were observed in these cases.

1. Introduction

The salen (bis(salicylaldehydo)ethylenediamine) and salen-type ligands with various metal centers comprise a highly active class of synthetic complexes.[1−4] Depending on the metal center (normally 3d- and 4d-metals), these complexes have been utilized for numerous asymmetric catalysis applications.[5−7] Research on the immobilization of the metal−salen complexes has shown that different schemes can greatly effect the catalytic activity.[8] The molecular supports, furthermore, may have a significant influence on the electronic structure of the metal−salen complexes.[9] Understanding the underlying catalytic reaction mechanisms via electronic structure computations could immensely aid past and ongoing efforts to tune the reactivity and selectivity of metal−salen catalysts.

Previous theoretical studies on metal−salen systems are largely limited to the Mn−salen complex[10−26] while very few have explored different metal centers with multireference methods.[27−29] Density functional theory (DFT) methods[30,31] have seen much success in its applications to organic chemistry and has become attractive for coordination chemistry as well.[32−37] However, currently popular density functional approximations can be less reliable for systems containing transition metals when several low-lying electronic states are present.[10,38−42] Furthermore, there exist benchmark studies of DFT computations on transition metal ligand complexes,[43−45] but few reach the size and complexity of the metal−salen systems. Of significant importance, the application of two common DFT methods on the olefin epoxidation mechanism with the Mn−salen catalyst yields large qualitative discrepancies.[11]

Transition metal complexes can feature strong dynamical and nondynamical electron correlation effects, which makes them difficult to describe theoretically. One possible solution is to include higher-order excitations in the treatment of electron correlation. Unfortunately, such approaches become computationally intractable for larger molecules. Another approach is to treat the system with multireference methods.[46−48] The difficulty of utilizing this approach is complicated by the selection of appropriate active spaces and the sufficient treatment of dynamical electron correlation. Work in our group on the d^0 and d^2 metal−salens[28,29] has outlined a procedure for the proper treatment of metal−salen complexes with minimal active space multireference methods and has shown that DFT methods, in general, fail to properly describe the singlet, triplet, and quintet energy gaps for a series of metal−salen complexes.

This work extends our systematic study on the accuracy of DFT methods to the d^6 metal−salen complexes. In particular, the Fe(II)−, Co(III)−, Ni(IV)−, Ru(II)−, Rh(III)−, and Pd(IV)−metal salen complexes are considered. Optimized geometries and relative energies obtained using various density functional approximations are benchmarked against high-level multireference ab initio methods. This work improves upon prior studies of d^0 and d^2 metal−salen complexes by considering both the smaller model salen ligand used previously and a larger model system. As before, this work is not intended to study the chemical properties of the metal−salen systems per se but to test the reliability of DFT methods for use in such studies. The d^6 metal−salen series does, however, contain important complexes utilized for catalytic transformations. The Ru(II)−salen has been shown to catalyze the cyclopropanation of olefins and the Co(III)−salen has been used to catalyze the hydrolytic kinetic resolution (HKR) reaction.[49−52] Furthermore, the efficiency of supported Co(III)−salen for HKR reactions has also been extensively studied.[8,9,53−55] The results presented here serve to guide future theoretical investigations on these highly important series of metal−salen catalysts.

* To whom correspondence should be addressed, sherrill@gatech.edu.

10.1021/jp903865t CCC: $40.75
Published on Web 07/21/2009

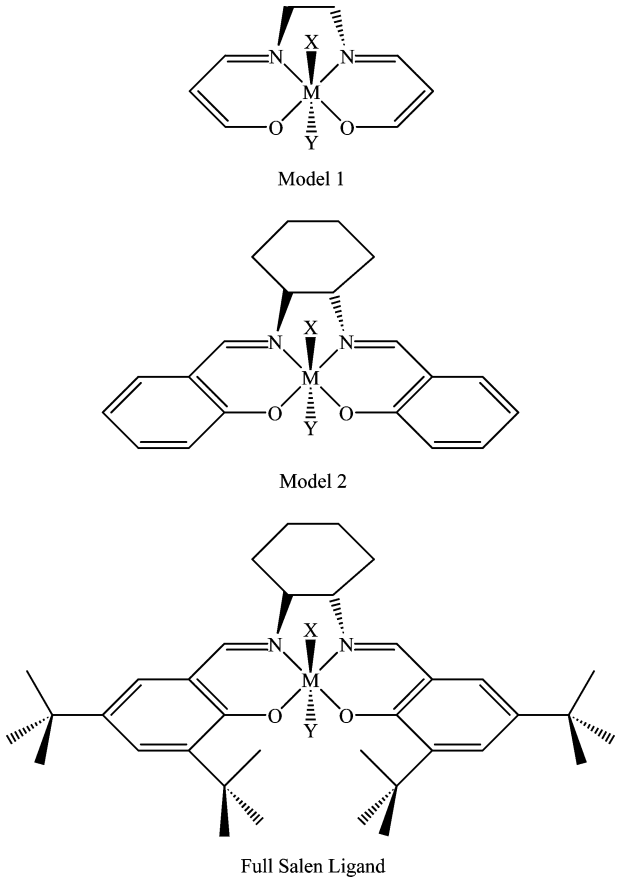

Figure 1. Two model systems for the metal−salen catalysts and the full salen ligand. Axial ligands may be present in positions X and Y; however, no axial ligands were considered in the present work.

2. Theoretical Methods

Figure 1 shows the two model systems for the metal−salens, as well as the full salen ligand. No axial ligands were used in this study in an attempt to focus on the nature of the interaction between the metal center and only the salen ligand. The metal centers, M, studied were Fe(II), Co(III), Ni(IV), Ru(II), Rh(III), and Pd(IV). All DFT computations were performed with the Jaguar 5.5 suite of programs.[56] The combination of Becke's 1988[57] exchange functional with Perdew's 1986[58] correlation functional (BP86) and the combination of Becke's three parameter hybrid functional[59] with the correlation functional of Lee, Yang, and Parr[60] (the hybrid functional, B3LYP) DFT methods were utilized with the Los Alamos basis sets and corresponding effective core potentials of Hay and Wadt (LANL2DZ) for all transition metal atoms[61] and the 6-31G* basis sets for all other atoms[62] (LANL2DZ*). The pseudospectral DFT implementation[63] with a fine grid, as found in Jaguar 5.5, was used to completely optimize the geometries (root-mean-square (rms) gradient 10^{-3} au) for the lowest singlet, triplet, quintet states of each functional for each model system. A restricted open-shell reference was used in DFT computations of triplet and quintet states. Frequency computations were performed to ensure the structures corresponded to potential energy minima.

All complete active-space (CAS) type methods were performed with the MOLPRO 2006.1 package of ab initio programs.[64] The converged BP86 geometries were used as starting points for the complete active-space self-consistent field (CASSCF)[47] optimizations of the model 1 complexes. Starting orbitals were generated using the configuration of singles and doubles (CISD) method with the STO-3G[65−67] basis sets. Large CAS-configuration interaction (CAS-CI)[48] computations were performed with the CISD natural orbital guesses. The active spaces were chosen from an examination of the most important orbitals in the CAS-CI vector. From this starting information, the final CASSCF wave functions were determined using the LANL2DZ* basis. For the model 2 systems, CASSCF single-point computations were performed for the Fe(II)−, Co(III)−, Ru(II)−, and Rh(III)−salens at the optimized B3LYP model 2 geometries.

CAS second-order and third-order perturbation theory (CASPT2[68,69] and CASPT3)[70] methods were performed at the converged CASSCF geometries (rms gradient 10^{-3} au) for the model 1 systems. Due to the limitation on the number of correlated orbitals that can be included in the CASPT3 program, the lowest 27 molecular orbitals were frozen throughout the CASPT3 computations. Estimates of the full CASPT3 energies were obtained by correcting the internally contracted CASPT2 energies with the difference between CASPT3 and CASPT2 with the 27 lowest orbitals frozen. All computations employed a restricted-core approximation with a small-core, 1s2s2p3s and 1s2s2p3s3p3d4s for the 3d and 4d transition metals, respectively. The leading determinants from the CASSCF CI expansions indicated the degree of multireference character for each complex.

Optimized model 1 CASSCF geometries were compared to optimized model 1 DFT geometries and the least root mean squared deviation (LRMSD) values were computed with the Visual Molecular Dynamics (VMD) program.[71] Similarly, the LMRSDs were calculated between the optimized model 1 B3LYP geometries and the opimized model 2 B3LYP geometries, where only the heavy atoms of the model 1 systems and the corresponding atoms of the model 2 systems were compared. Molecular orbital isosurfaces were generated using MOLEKEL with contour values of 0.05.[72]

3. Results and Discussion

Table 1 provides the relative energies for the singlet, triplet, and quintet states for the model 1 and 2 Fe(II)−, Co(III)−, Ru(II)−, and Rh(III)−salens, and the model 1 Ni(IV)− and Pd(IV)−salens. States that are nearly isoenergetic with the lowest states provided in Table 1 and explicit geometry analyses are not presented here for the sake of brevity and can be found in the Supporting Information along with the CASSCF, B3LYP, and BP86 optimized geometries.

Figure 2 shows a representation of the active space orbitals used in the CAS-type computations. The computed active space orbitals match our chemical intuition in that the highest lying occupied and partially occupied molecular orbitals are the five non/antibonding d-orbitals of the metal center. Our previous work, furthermore, outlines the importance of the two C−C−C (three-center, two-electron) π bonds referred to as Rπ_1 and Rπ_2 hereafter. In Figure 2, both Rπ_1 and Rπ_2 are represented by the Rπ orbital plot. These Rπ orbitals are included only for the Ni(IV)− and Pd(IV)−salens leading to active spaces consisting of 10 electrons in 7 orbitals. This is due to the increased positive charge on the metal center compared to other metal−salens considered, which lowers the energy of the d orbitals relative to that of the Rπ orbitals. For the Fe(II)−, Co(III)−, Ru(II)−, and Rh(III)−salens, the Rπ_1 and Rπ_2 orbitals remain doubly occupied leading to active spaces consisting of 6 electrons in 5 orbitals. In general, the bonding nature of the metal center with the salen ligand mainly relies on the interactions between the d_{xy} metal orbital with the p orbitals of the surrounding nitrogen

TABLE 1: Relative Energies (kcal mol^{-1}) for the Low-Lying Electronic States of the Model 1 and Model 2 (in Parentheses) d^6-Metal−Salens Computed at Various Levels of Theory

	state	CASPT3[a]	CASPT2[a]	CASSCF	B3LYP	BP86
Fe(II)	1^1A	56.17	61.42	69.72 (79.86)	28.78 (28.00)	16.60 (15.48)
	1^3A	21.90	25.43	36.30 (41.06)	0.00 (1.33)	0.00 (0.00)
	1^5A	0.00	0.00	0.00 (0.00)	3.91 (0.00)	15.55 (11.82)
Co(III)	1^1A	33.54	41.07	46.56 (43.79)	12.36 (13.08)	0.48 (1.06)
	1^3A	0.00	1.76	9.93 (10.97)	0.00 (0.00)	0.00 (0.00)
	1^5A	21.43	0.00	0.00 (0.00)	15.39 (11.93)	24.78 (22.27)
Ni(IV)	1^1A	1.13	0.81	0.61	0.00	0.00
	1^3A	0.41	0.25	0.00	20.88	8.97
	1^5A	0.00	0.00	0.06	8.24	39.40
Ru(II)	1^1A	22.61	22.44	26.06 (32.63)	10.18 (8.09)	2.48 (15.48)
	1^3A	0.00	0.00	0.00 (2.85)	0.00 (0.00)	0.00 (0.00)
	1^5A	14.69	10.09	3.33 (0.00)	37.62 (34.43)	46.77 (36.95)
Rh(III)	1^1A	17.42	11.75	22.34 (24.49)	0.00 (0.00)	0.00 (0.00)
	1^3A	0.00	0.00	0.00 (0.00)	2.91 (2.79)	8.69 (6.98)
	1^5A	63.11	24.45	35.96 (29.68)	49.03 (45.74)	58.48 (54.26)
Pd(IV)	1^1A	0.00	0.00	0.00	4.84	0.00
	1^3A	0.41	0.47	0.14	0.00	6.53
	1^5A	29.08	26.07	13.24	43.35	51.57

[a] Relative energies computed at the CASSCF optimized geometries.

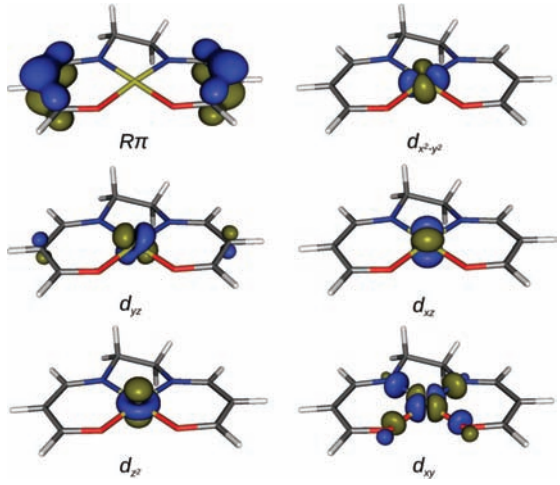

Figure 2. Representation of the active space orbitals for the d^6 metal−salen catalysts.

TABLE 2: Leading Determinants in the Natural Orbital Basis from SA-CASSCF Calculations on the Low-Lying Electronic States of Fe(II)− and Ru(II)−Salens

	state	determinant	coeff
Fe(II)	1^1A	$(d_{x^2-y^2})^2\ (d_{xz})^2\ (d_{z^2})\beta\ (d_{yz})\alpha$	0.663
		$(d_{x^2-y^2})^2\ (d_{xz})^2\ (d_{z^2})\alpha\ (d_{yz})\beta$	−0.663
		$(d_{x^2-y^2})^2\ (d_{xz})^2\ (d_{z^2})^2$	−0.165
	1^3A	$(d_{x^2-y^2})^2\ (d_{xz})\alpha\ (d_{z^2})^2\ (d_{yz})\alpha$	0.976
		$(d_{x^2-y^2})^2\ (d_{xz})\alpha\ (d_{yz})\alpha\ (d_{xy})^2$	−0.116
	1^5A	$(d_{x^2-y^2})\alpha\ (d_{xz})\alpha\ (d_{z^2})^2\ (d_{yz})\alpha\ (d_{xy})\alpha$	0.986
		$(d_{x^2-y^2})^2\ (d_{xz})\alpha\ (d_{z^2})\alpha\ (d_{yz})\alpha\ (d_{xy})\alpha$	−0.164
Ru(II)	1^1A	$(d_{x^2-y^2})^2\ (d_{xz})^2\ (d_{z^2})^2$	0.795
		$(d_{x^2-y^2})^2\ (d_{xz})^2\ (d_{yz})^2$	−0.334
		$(d_{x^2-y^2})^2\ (d_{z^2})^2\ (d_{yz})^2$	−0.268
		$(d_{x^2-y^2})\beta\ (d_{xz})^2\ (d_{z^2})\alpha\ (d_{yz})^2$	−0.254
		$(d_{x^2-y^2})\alpha\ (d_{xz})^2\ (d_{z^2})\beta\ (d_{yz})^2$	0.254
	1^3A	$(d_{x^2-y^2})^2\ (d_{xz})^2\ (d_{z^2})\alpha\ (d_{yz})\alpha$	0.925
		$(d_{x^2-y^2})\alpha\ (d_{xz})^2\ (d_{z^2})^2\ (d_{yz})\alpha$	0.366
	1^5A	$(d_{x^2-y^2})\alpha\ (d_{xz})\alpha\ (d_{z^2})^2\ (d_{yz})\alpha\ (d_{xy})\alpha$	0.741
		$(d_{x^2-y^2})^2\ (d_{xz})\alpha\ (d_{z^2})\alpha\ (d_{yz})\alpha\ (d_{xy})\alpha$	−0.624
		$(d_{x^2-y^2})\alpha\ (d_{xz})\alpha\ (d_{z^2})\alpha\ (d_{yz})^2\ (d_{xy})\alpha$	0.248

and oxygen atoms. The antibonding d_{xy} orbital, accordingly, is always the highest lying among the active space d orbitals.

3.1. Fe(II)− and Ru(II)−Salens. For the neutral Fe(II)− and Ru(II)−salens, the active spaces chosen were comprised of the five d-orbitals. CAS-type computations for the Fe(II)−salen predict a quintet ground state followed by a triplet state and then a singlet state, 22 and 56 kcal mol^{-1} higher in energy relative to the quintet state, respectively, for the CASPT3 method. Both DFT methods predict a triplet ground state followed by a quintet state. For the Ru(II)−salen, all methods predict a triplet ground state. The energetic orderings, however, are not consistent. The CASPT3 method indicates the quintet state to be 15 kcal mol^{-1} above the triplet state and a singlet state 8 kcal mol^{-1} higher than the quintet state. The B3LYP method predicts the singlet state to follow the triplet state with a relative energy of 10 kcal mol^{-1} and then the quintet state 28 kcal mol^{-1} higher than the singlet state. The BP86 relative energies show the same trend as the B3LYP relative energies.

The discrepancy between the DFT and CAS-type methods can be rationalized by examining the leading determinants from CASSCF computations (a representative example is shown in Table 2). The small coefficients of the most important determinants indicate the high degree of multireference character of the Fe(II)− and Ru(II)−salen wave functions. For example, the largest determinant in the Fe(II)−salen singlet state CI wave function is only 0.663. By contrast, wave functions dominated by a single reference typically have a leading CI coefficient of about 0.9 or larger. The CI wave functions are consistent with near degeneracies of the $d_{x^2-y^2}$, d_{xz}, d_{z^2}, and d_{yz} orbitals. The d_{xy} orbital is higher in energy, however, with a small energy gap in the Fe(II)−salen (which favors the high-spin quintet state) and a somewhat larger energy gap in the Ru(II)−salen (which favors the triplet state). The orbital degeneracies make the Fe(II)− and Ru(II)−salens difficult to describe with the B3LYP and BP86 DFT methods. This strong multireference character continues throughout the d^6 metal−salen series.

3.2. Co(III)− and Rh(III)−Salens. As with the Fe(II)− and Ru(II)−salens, the active space chosen for the Co(III)− and Rh(III)−salens was comprised of the five d-orbitals. Interestingly for the Co(III)−salen, the CASPT3 and DFT methods predict a triplet ground state, and the CASPT2 and CASSCF methods predict a quintet ground state. As the higher-order perturbations are added to the CASSCF computations, the triplet and quintet states become nearly degenerate, as predicted by the CASPT2 method, and eventually switch order as in the CASPT3 computations. The corrections, however, do not seem to be

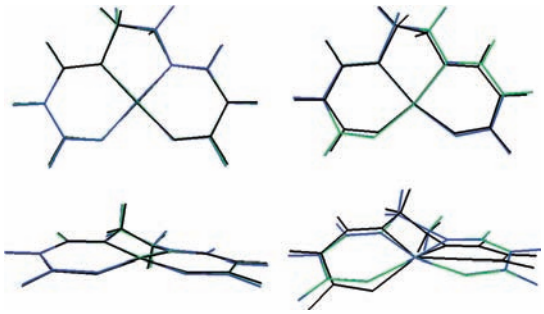

Figure 3. Overlay of the CASSCF (black), B3LYP (green), and BP86 (blue) optimized geometries for the 1^1A (left) and 1^5A (right) states of Co(III)−salen.

convergent. The difference in relative energies for the CASSCF triplet and quintet states is ∼10 kcal mol^{-1}. This difference changes to ∼2 kcal mol^{-1} and then ∼21 kcal mol^{-1} for the CASPT2 and CASPT3 triplet and quintet states, respectively. This trend makes it difficult to assess the performance of DFT methods because, in this case, the CAS-type computations do not appear to have converged.

3.3. Ni(IV)− and Pd(IV)−Salens. The charge of the metals in Ni(IV)−salen and Pd(IV)−salen pulls electron density toward the center. Consequently, the active spaces for the Ni(IV)− and Pd(IV)−salens were increased to include both Rπ orbitals as well as the five d-orbitals, whereas in the previous metal−salens the Rπ orbitals always remained doubly occupied. CAS-type relative energies for the Ni(IV)−salen suggest that the lowest singlet, triplet, and quintet states are nearly degenerate. Both DFT methods predict an apparent singlet ground state; however, the ordering of the other states is in disagreement. The B3LYP method predicts a quintet state to follow the singlet state with a relative energy of 8 kcal mol^{-1} and the triplet state 13 kcal mol^{-1} higher than the quintet state. The BP86 method, on the other hand, predicts the triplet state to follow the singlet state with a relative energy of 9 kcal mol^{-1} and the quintet state 30 kcal mol^{-1} higher than the triplet state. For the Pd(IV)−salen, CAS-type computations predict nearly degenerate singlet and triplet states with a high lying quintet state (29 kcal mol^{-1} above the ground state according to the CASPT3 method). Both DFT methods, in this case, are in agreement with the CAS-type methods, but with overestimations of the quintet energies (43 and 52 kcal mol^{-1} for the B3LYP and BP86 methods, respectively). This could be due to either the overstabilization of the low spin states or the understabilization of the quintet states.

3.4. Geometry Analyses. Although the energetic ordering of states does not appear reliable as computed by DFT methods, DFT optimized geometries are in good agreement with CASSCF optimized geometries; errors are mostly on the order of 0.1 Å LMRSD. Figure 3 overlays the DFT geometries with the CASSCF geometries for the singlet and quintet states of Co(III)−salen. The worst agreement between the DFT and CASSCF methods for geometries is observed for the quintet state of the Co(III)−salen, where there is a deviation of 0.3 Å LRMSD. LMRSDs over 0.2 Å for DFT methods normally appear when comparing the quintet states of the metal−salens (specifically the Ru(II)−, Co(III)−, and Pd(IV)−salens). The salen ligands in the quintet state CASSCF geometries twist out of planarity to a greater degree than the lower spin state geometries as depicted in Figure 3. DFT methods do not predict this out of plane twisting for the quintet states. Uncharacteristically, DFT singlet state optimized geometries for the Ni(IV)−salen incur greater deviations (∼0.24 Å LMRSDs) than the higher spin state geometries compared to CASSCF optimized geometries. For all other metal−salens considered, the largest deviations are between the quintet geometries. Nevertheless, the DFT and CASSCF optimized geometries are fairly similar for all systems considered.

TABLE 3: LRMSD (Å) in Molecular Geometries[a] for the Optimized 1^1A, 1^3A, and 1^5A States for the B3LYP Model 1 Compared to Model 2 Systems

	state	LRMSD
Fe(II)	1^1A	0.23
	1^3A	0.05
	1^5A	0.19
Co(III)	1^1A	0.20
	1^3A	0.06
	1^5A	0.14
Ru(II)	1^1A	0.33
	1^3A	0.06
	1^5A	0.24
Rh(III)	1^1A	0.08
	1^3A	0.06
	1^5A	0.10

[a] Comparisons based on the heavy atoms of the model 1 system.

3.5. Larger Model Salens. Due to the reliable performance of DFT optimizations, CASSCF computations for the model 2 salens were performed at B3LYP optimized geometries. The relative energies for the model 2 Fe(II)−, Co(III)−, Ru(II)−, and Rh(III)−salens are shown in parentheses in Table 1. All methods predict the same energetic trends for the model 2 systems as for the model 1 systems. The similar trends indicate that there are no dramatic changes in the electronic structure as the larger model systems are used. This result is expected since the most important orbitals are the d-orbitals of the metal center and it is unlikely that they will mix to a significant degree when moving from the model 1 to the model 2 system. For the model 2 Ni(IV)− and Pd(IV)−salens, difficulties in keeping the appropriate orbitals within the active spaces for the CASSCF computations were encountered. It remains unknown whether the differences between the Rπ orbitals of the model 1 and model 2 systems change the energetic ordering of spin states and the energy gaps between them for these two cases.

The B3LYP optimized geometry LMRSDs between the model 1 and 2 systems are presented in Table 3. For all triplet geometries considered, the model 1 systems are very similar to the model 2 systems with 0.06 Å LMRSDs or less. The optimized Rh(III)−salen model 1 geometries reproduce the model 2 geometries for the singlet, triplet, and quintet states to less than 0.10 Å LMRSD. The comparison of the Ru(II)−salen singlet geometries incurs the greatest error of 0.33 Å LMRSD. Although some of the model 1 geometries differ by a few tenths of Å LMRSDs compared to the model 2 geometries, they are close enough to capture the correct electronic structure of the complexes considered here. Moreover, preliminary investigations suggest that the model 2 ligand does a good job reproducing the geometry of the full salen ligand.

4. Conclusions

The systematic study of the reliability of DFT methods for organometallic complexes has been extended to the d^6 metal−salens. DFT methods rarely predict the correct ordering of states as compared to high-level CASPT3 results. Moreover, in general, the splitting between states seems to be underestimated by the B3LYP and BP86 functionals.

For the highly charged Ni(IV)− and Pd(IV)−salens, however, either the quintet states are understabilized or the singlet and

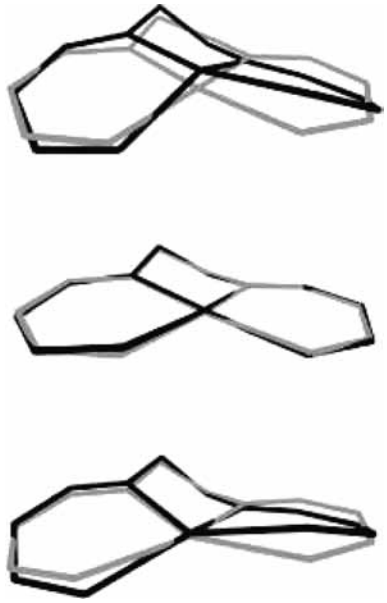

Figure 4. Overlay of the model 2 (black) and model 1 (gray) B3LYP optimized geometries (common heavy atoms only) for the 1^1A (top), 1^3A (center), and 1^5A (bottom) states of Ru(II)−salen.

triplet spin states are overstabilized, which leads to overestimated energy gaps. A curious nonconvergence of the perturbative correction series for the Co(III)− and Rh(III)−salens was observed. Further investigation of these systems is underway.

Unfortunately, we have not detected a trend which would indicate when DFT can be expected to provide reliable energetic ordering of spin states for metal−salen complexes. However, DFT geometry optimizations are in good agreement with CASSCF geometry optimizations. This result is consistent with previous findings for d^0 and d^2 metal−salen complexes. The results for the energetic ordering of spin states for the larger model 2 salen, furthermore, show no appreciable difference from the smaller model 1 salen results. Therefore, the model 1 system and DFT geometry optimizations can be considered appropriate for most computations concerning d^6 metal−salens. New DFT functionals may improve the accuracy and reliability when considering metal−ligand complexes[33,73,74] and as such, further research is necessary and is currently underway.

Acknowledgment. This material is based upon work supported by the U.S. Department of Energy, Basic Energy Sciences (Catalysis Science Grant/Contract No. DE-FG02-03ER15459).

Supporting Information Available: Listings of relative energies of metal−salen complexes. This material is available free of charge via the Internet at http://pubs.acs.org.

References and Notes

(1) Yoon, T. P.; Jacobsen, E. N. *Science* **2003**, *299*, 1691–1693.
(2) Katsuki, T. *Adv. Synth. Catal.* **2002**, *344*, 131–147.
(3) Noyori, R. *Adv. Synth. Catal.* **2003**, *345*, 15–32.
(4) Blaser, H. U.; Spindler, F.; Studer, A. *Appl. Catal., A* **2001**, *221*, 119–143.
(5) Venkataramanan, N. S.; Kuppuraj, G.; Rajagopal, S. *Coord. Chem. Rev.* **2005**, *249*, 12491268.
(6) McGarrigle, E. M.; Gilheany, D. G. *Chem. Rev.* **2005**, *105*, 1563–1602.
(7) Canali, L.; Sherrington, D. C. *Chem. Soc. Rev.* **1999**, *28*, 85–93.
(8) Zheng, X. L.; Jones, C. W.; Weck, M. *Chem.−Eur. J.* **2005**, *12*, 576–583.
(9) Zheng, X. L.; Jones, C. W.; Weck, M. *J. Am. Chem. Soc.* **2007**, *129*, 1105–1112.
(10) Sears, J. S.; Sherrill, C. D. *J. Chem. Phys.* **2006**, *124*, 144314.
(11) Cavallo, L.; Jacobsen, H. *J. Phys. Chem. A* **2003**, *107*, 5466.
(12) Strassner, T.; Houk, K. N. *Org. Lett.* **1999**, *1*, 419–421.
(13) Khavrutskii, I. V.; Musaev, D. G.; Morokuma, K. *Proc. Natl. Acad. Sci. U.S.A.* **2004**, *101*, 5743–5748.
(14) Jacobsen, H.; Cavallo, L. *Phys. Chem. Chem. Phys.* **2004**, *6*, 3747–3753.
(15) Ivanic, J. *J. Chem. Phys.* **2003**, *119*, 9377–9385.
(16) Abashkin, Y. G.; Collins, J. R.; Burt, S. K. *Inorg. Chem.* **2001**, *40*, 4040–4048.
(17) Khavrutskii, I. V.; Musaev, D. G.; Morokuma, K. *Inorg. Chem.* **2005**, *44*, 306–315.
(18) Khavrutskii, I. V.; Rahim, R. R.; Musaev, D. G.; Morokuma, K. *J. Phys. Chem. B* **2004**, *108*, 3845–3854.
(19) Khavrutskii, I. V.; Musaev, D. G.; Morokuma, K. *J. Am. Chem. Soc.* **2003**, *125*, 13879–13889.
(20) Linde, C.; Arnold, M.; Norrby, P. O.; Akermark, B. *Angew. Chem., Int. Ed.* **1997**, *36*, 1723–1725.
(21) Linde, C.; Arnold, M.; Norrby, P. O.; Akermark, B.; Svensson, M. *J. Am. Chem. Soc.* **1999**, *121*, 5083–5084.
(22) Jacobsen, H.; Cavallo, L. *Chem.−Eur. J.* **2001**, *7*, 800–807.
(23) Cavallo, L.; Jacobsen, H. *Inorg. Chem.* **2004**, *43*, 2175–2182.
(24) Cavallo, L.; Jacobsen, H. *J. Org. Chem.* **2003**, *68*, 6202–6207.
(25) Cavallo, L.; Jacobsen, H. *Angew. Chem., Int. Ed.* **2000**, *39*, 589–592.
(26) Abashkin, Y. G.; Burt, S. K. *Org. Lett.* **2004**, *6*, 59–62.
(27) Ivanic, J.; Collins, J. R.; Burt, S. K. *J. Phys. Chem. A* **2004**, *108*, 2314–2323.
(28) Sears, J. S.; Sherrill, C. D. *J. Phys. Chem. A* **2008**, *112*, 6741–6752.
(29) Sears, J. S.; Sherrill, C. D. *J. Phys. Chem. A* **2008**, *112*, 3466–3477.
(30) Kohn, W.; Sham, L. J. *Phys. Rev.* **1965**, *140*, 1133.
(31) Hohenberg, P.; Kohn, W. *Phys. Rev. B* **1964**, *136*, B864.
(32) Chermette, H. *Coord. Chem. Rev.* **1998**, *178*, 699–721.
(33) Zhao, Y.; Truhlar, D. G. *J. Chem. Phys.* **2006**, *125*, 194101.
(34) Vlček, A.; Zàliš, S. *Coord. Chem. Rev.* **2007**, *251*, 258–187.
(35) Schäffer, C. E.; Anthon, C.; Bendix, J. *Coord. Chem. Rev.* **2009**, *253*, 575–593.
(36) Anthon, C.; Bendix, J.; Schäffer, C. E. *Inorg. Chem.* **2004**, *43*, 7882–7886.
(37) Petrie, S.; Stranger, R. *Inorg. Chem.* **2003**, *43*, 2597–2610.
(38) Yanagisawa, S.; Tsuneda, T.; Hirao, K. *J. Chem. Phys.* **2000**, *112*, 545–553.
(39) Barden, C. J.; Rienstra-Kiracofe, J. C.; Schaefer, H. F. *J. Chem. Phys.* **2000**, *113*, 690–700.
(40) Nakao, Y.; Hirao, K.; Taketsugu, T. *J. Chem. Phys.* **2001**, *114*, 7935–7940.
(41) Harvey, J. N. *Struct. Bonding (Berlin)* **2004**, *121*, 151–183.
(42) Ghosh, A. *J. Biol. Inorg. Chem.* **2006**, *11*, 712–724.
(43) Zhao, Y.; Truhlar, D. G. *J. Chem. Phys.* **2006**, *124*, 224105.
(44) Quintal, M. M.; Karton, A.; Iron, M. A.; Boese, A. D.; Martin, J. M. L. *J. Phys. Chem. A* **2006**, *110*, 709–716.
(45) Wang, S. G.; Schwarz, W. H. E. *J. Chem. Phys.* **1998**, *109*, 7252–7262.
(46) Schmidt, M. W.; Gordon, M. S. *Annu. Rev. Phys. Chem.* **1998**, *49*, 233–266.
(47) Roos, B. O.; Taylor, P. R.; Siegbahn, P. E. M. *Chem. Phys.* **1980**, *48*, 157.
(48) Sherrill, C. D.; Schaefer, H. F. *Adv. Quantum Chem.* **1999**, *34*, 143–269.
(49) Cozzi, P. G. *Chem. Soc. Rev.* **2004**, *33*, 410–421.
(50) Madhavan, N.; Jones, C. W.; Weck, M. *Acc. Chem. Res.* **2008**, *41*, 1153–1165.
(51) Schaus, S. E.; Brandes, B. D.; Larrow, J. F.; Tokunaga, M.; Hansen, K. B.; Gould, A. E.; Furrow, M. E.; Jacobsen, E. N. *J. Am. Chem. Soc.* **2002**, *124*, 1307–1315.
(52) Larrow, J. F.; Hemberger, K. E.; Jasmin, S.; Kabir, H.; Morel, P. *Tetrahedron: Asymmetry* **2003**, *14*, 3589–3592.
(53) Jain, S.; Zheng, X. L.; Jones, C. W.; Weck, M.; Davis, R. J. *Inorg. Chem.* **2007**, *21*, 8887–8896.
(54) Zheng, X. L.; Jones, C. W.; Weck, M. *Adv. Synth. Catal.* **2008**, *350*, 255–261.
(55) Gill, C. S.; Venkatasubbaiah, K.; Phan, N. T. S.; Weck, M.; Jones, C. W. *Chem.−Eur. J.* **2008**, *14*, 7306–7313.
(56) *Jaguar, version 5.5*; Schrödinger LLC, 1991−2003.
(57) Becke, A. D. *Phys. Rev. A* **1988**, *38*, 3098–3100.
(58) Perdew, J. P. *Phys. Rev. B* **1986**, *33*, 8822–8824.
(59) Becke, A. D. *J. Chem. Phys.* **1993**, *98*, 1372–1377.
(60) Lee, C.; Yang, W.; Parr, R. G. *Phys. Rev. B* **1988**, *37*, 785–789.
(61) Hay, P. J.; Wadt, W. R. *J. Chem. Phys.* **1985**, *82*, 270–283.
(62) Francl, M. M.; Pietro, W. J.; Hehre, W. J.; Binkley, J. S.; Gordon, M. S.; Defrees, D. J.; Pople, J. A. *J. Chem. Phys.* **1982**, *77*, 3654–3665.

(63) Chasman, D.; Beachy, M. D.; Wang, L. M.; Friesner, R. A. *J. Comput. Chem.* **1998**, *19*, 1017–1029.

(64) Werner, H.-J.; Knowles, P. J.; Lindh, R.; Manby, F. R.; Schütz, M.; Celani, P.; Korona, T.; Rauhut, G.; Amos, R. D.; Bernhardsson, A.; Berning, A.; Cooper, D. L.; Deegan, M. J. O.; Dobbyn, A. J.; Eckert, F.; Hampel, C.; Hetzer, G.; Lloyd, A. W.; McNicholas, S. J.; Meyer, W.; Mura, M. E.; Nicklass, A.; Palmieri, P.; Pitzer, R.; Schumann, U.; Stoll, H.; Stone, A. J.; Tarroni, R.; Thorsteinsson, T. *Molpro, version 2006.1, a package of ab initio programs*, 2006. See http://www.molpro.net.

(65) Hehre, W. J.; Stewart, R. F.; Pople, J. A. *J. Chem. Phys.* **1969**, *51*, 2657–2664.

(66) Hehre, W. J.; Ditchfie, R.; Stewart, R. F.; Pople, J. A. *J. Chem. Phys.* **1970**, *52*, 2769.

(67) Pietro, W. J.; Hehre, W. J. *J. Comput. Chem.* **1983**, *4*, 241–251.

(68) Celani, P.; Werner, H.-J. *J. Chem. Phys.* **2000**, *112*, 5546–5557.

(69) Andersson, K.; Malmqvist, P.-Å.; Roos, B. O.; Sadlej, A. J.; Wolinski, K. *J. Phys. Chem.* **1990**, *94*, 5483–5488.

(70) Werner, H. J. *Mol. Phys.* **1996**, *89*, 645–661.

(71) Humphrey, W.; Dalke, A.; Schulten, K. *J. Mol. Graphics Modell.* **1996**, *14*, 33.

(72) Portmann, S.; Luthi, H. P. *Chimia* **2000**, *54*, 766–770.

(73) Zhao, Y.; Schultz, N. E.; Truhlar, D. G. *J. Chem. Theory Comput.* **2006**, *2*, 364–382.

(74) Zhao, Y.; Truhlar, D. G. *Theor. Chem. Acc.* **2008**, *120*, 215–241.

JP903865T